Inorganic Chemistry

Article

pubs.acs.org/IC

Stretch Out or Fold Back? Conformations of Dinuclear Gold(I) *N*-Heterocyclic Carbene Macrocycles

Stefanie Kobialka,[†] Christina Müller-Tautges,[†,#] Melanie T. S. Schmidt,[†] Gregor Schnakenburg,[†] Oldamur Hollóczki,[‡] Barbara Kirchner,[‡] and Marianne Engeser*[,†]

[†]Kekulé-Institute for Organic Chemistry and Biochemistry, University of Bonn, Gerhard-Domagk-Strasse 1, 53121 Bonn, Germany

[‡]Mulliken Center for Theoretical Chemistry, University of Bonn, Beringstrasse 4, 53115 Bonn, Germany

Supporting Information

ABSTRACT: We report the synthesis and characterization of 12 new dinuclear gold(I) N-heterocyclic carbene (NHC) complexes and the corresponding imidazolium precursors. The focus lies in a systematic study of conformational changes and intra- and intermolecular gold−gold and $\pi-\pi$ interactions of dinuclear gold(I) carbene complexes. Common to all members of the series of gold macrocycles are NHC ligands on the basis of imidazole with ethyl side chains and bromide as well as hexafluorophosphate counterions, respectively. The compounds vary in the length of a flexible alkyl linker between the NHC units. For the methylene and ethylene bridged macrocycles, a ring inversion movement can be observed by VT-NMR. In total, 11 molecular structures have been characterized by X-ray diffraction. Open ring conformations with intermolecular $\pi-\pi$ and Au−Au interactions prevail, but a backfolded conformation with a short intramolecular Au−Au distance has been found for the ethylene-bridged species. The presence of Au−Au interactions could be proven by quantum chemical calculations.

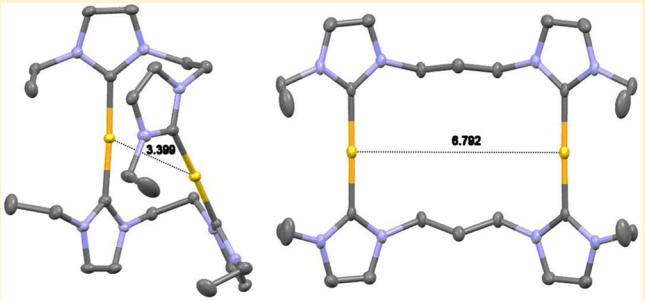

INTRODUCTION

In recent years, there has been an increasing interest in gold complexes with N-heterocyclic carbene (NHC) ligands[1] as a consequence of their promising applications in fields such as catalysis,[2] nanotechnology,[3,4] and medicine.[5−7] Given the usual linear coordination mode of Au^{I}, mononuclear gold(I) NHC compounds[1−6] often possess two different ligands (typically a neutral carbene and a coordinating anion).[1,8−11] The respective homoleptic derivates bearing two identical NHC ligands usually are cationic bis(NHC) gold(I) complexes.[4,8,9,11−17] The two NHC ligands can be connected with a long linker.[18,19] With shorter linkers, dinuclear macrocycles are formed which consist of two gold(I) atoms and two bridging bis(NHC) ligands.[19−29] A growing number of such homoleptic dinuclear gold(I) tetra(NHC) macrocycles have been reported in recent years, including compounds with very rigid[23,29b,d] and very flexible[19,22,24,26] linkers connecting the carbene subunits. Even a direct N−N connection of two NHC moieties is possible and results in an extremely short gold−gold distance.[27] A chiral example[25] as well as neutral macrocycles with anionic linkers[20,28] have been synthesized. Some multinuclear complexes with NHC-ligated Au^{I} atoms are also known.[30]

A very intriguing feature of gold(I) complexes is the occurrence of aurophilic interactions often recognized in the solid state by an intermetallic distance shorter than the sum of the van der Waals radii (3.5 Å).[31] The strength of this unusual bonding type is comparable to hydrogen bonds (5−10 kcal/mol).[31,32] The phenomenon has been associated with exceptional photophysical properties of gold compounds.[33,34] Mononuclear gold(I) complexes realize short Au−Au distances by intermolecular aggregation,[31] whereas dinuclear complexes can also adopt backfolded conformations with intramolecular Au−Au bonds.[1,31]

We are fascinated by the subtle interplay of weak interactions governing the conformation of gold(I) macrocycles. Thus, we now report the synthesis and characterization of a systematic series of new dinuclear gold(I) NHC complexes and their corresponding NHC precursors. The series consists of gold(I) complexes with N-heterocyclic carbene ligands on the basis of imidazole with ethyl side chains. The compounds only vary in the length of the alkyl chain linking two NHC units, respectively. Flexible alkyl linkers were chosen to systematically study the influence of the linker length on the conformation of the gold macrocycles with special respect to the formation of intramolecular gold−gold bonds. The synthesis and spectroscopical characterization of a related series of flexible gold(I) NHC macrocycles with methyl substituted carbenes has recently been reported, but only one substance thereof has been structurally characterized.[19,26a] This member of the series bears a propylene linker and shows an exceptionally efficient luminescence.[26a] Its structure reveals a backfolded conformation with short Au−Au distance irrespective of the anion (triflate[19] and hexafluorophosphate[26a]). Furthermore, two

Received: November 19, 2014
Published: June 18, 2015

DOI: 10.1021/ic502751s
Inorg. Chem. 2015, 54, 6100−6111

Scheme 1. Syntheses of the NHC Precursors 1−6 and the Dimeric Gold(I) Macrocycles 7−18

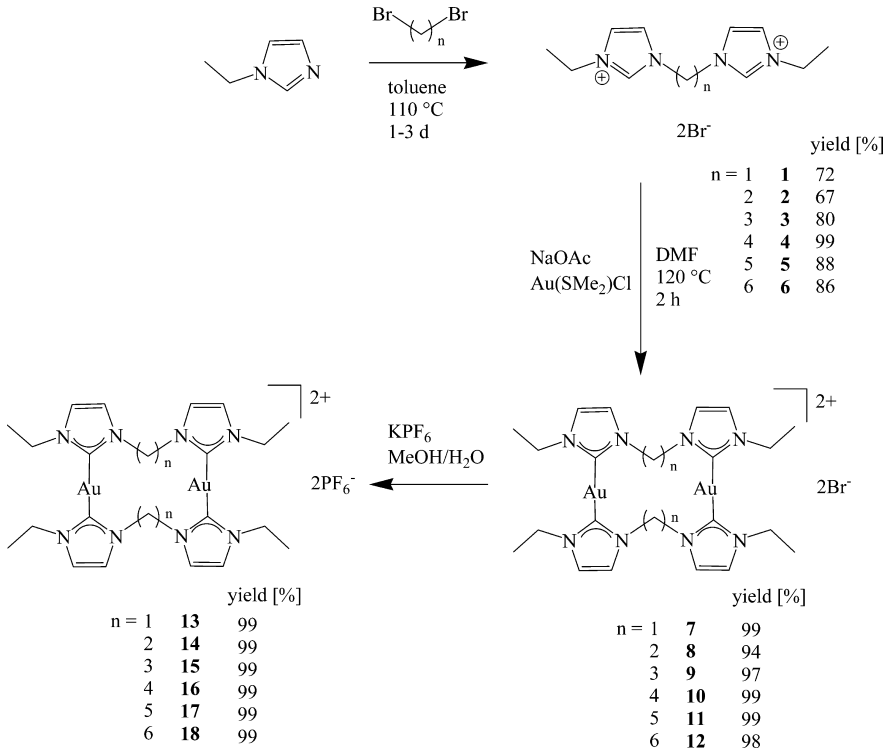

Scheme 2. Ring Inversion of Compounds 7/13.

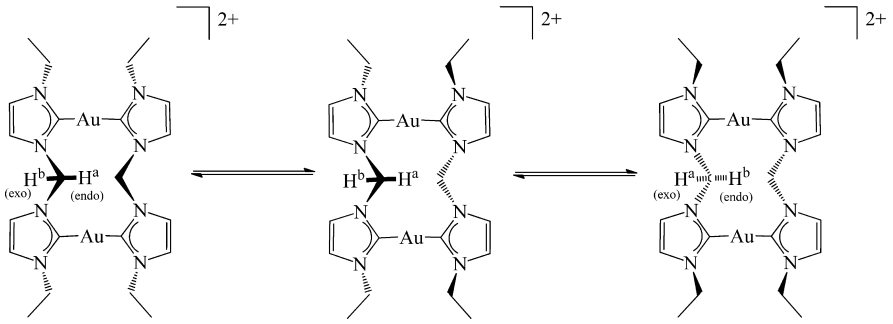

publications of the group of Hemmert may be combined to compare the first three members of a similar series with hydroxyl-functionalized side chains.[24] However, the anions affiliated with the reported molecular structures are not identical. This can have a disturbing impact on the observed conformations. We thus now report the spectroscopic characteristics and solid state molecular structures of the complete systematic ethyl series with alkyl linker lengths ranging from one to six methylene units. Both the counterions bromide and hexafluorophosphate have been investigated as the nature of the anion is known to have a severe impact on photoluminescent Au(I) complexes.[35]

RESULTS AND DISCUSSION

Synthesis. The ethyl imidazolium bromide salts **1**−**6**[36,37] (Scheme 1) were obtained by conversion of N-ethylimidazole with the corresponding alkyldibromide in toluene.[36] The corresponding NHC gold(I) bromide complexes **7**−**12** were synthesized by direct metalation of the respective imidazolium salt in the presence of sodium acetate in DMF according to a well-established procedure.[21,24,26] The complexes were purified by crystallization (slow diffusion of diethyl ether into a methanol solution). Subsequent anion exchange with KPF_6 in a methanol/water mixture gave the complexes **13**−**18** in excellent yields. The compounds **7**−**18** are readily characterized by electrospray (ESI) mass spectra showing intense signals for the intact dicationic macrocycle $[M]^{2+}$. We have not found indications for the presence of mononuclear complexes with a chelating bis-NHC-ligand known for longer linkers.[18,19]

NMR Spectroscopy. The room temperature ^1H and ^{13}C NMR spectra for the complexes **7**−**18** confirm the expected highly symmetrical structures. The formation of gold(I)-carbene complexes is accompanied by the disappearance of the acidic imidazolium proton signal at $\delta \approx 9.50$ ppm in the ^1H NMR spectrum and a typical shift of the $C_{carbene}$ signal from <140 ppm in the NHC precursor to >180 ppm in the gold(I) complex in the ^{13}C NMR spectrum.[1] In accordance to previously reported similar findings,[19,21a,24,26a] neither the exocyclic NHC side chain nor the counteranion induces significant changes in the macrocycle resonances at room temperature, whereas changing the solvent to acetonitrile induces a more pronounced upfield signal shift.

DOI: 10.1021/ic502751s
Inorg. Chem. 2015, 54, 6100−6111

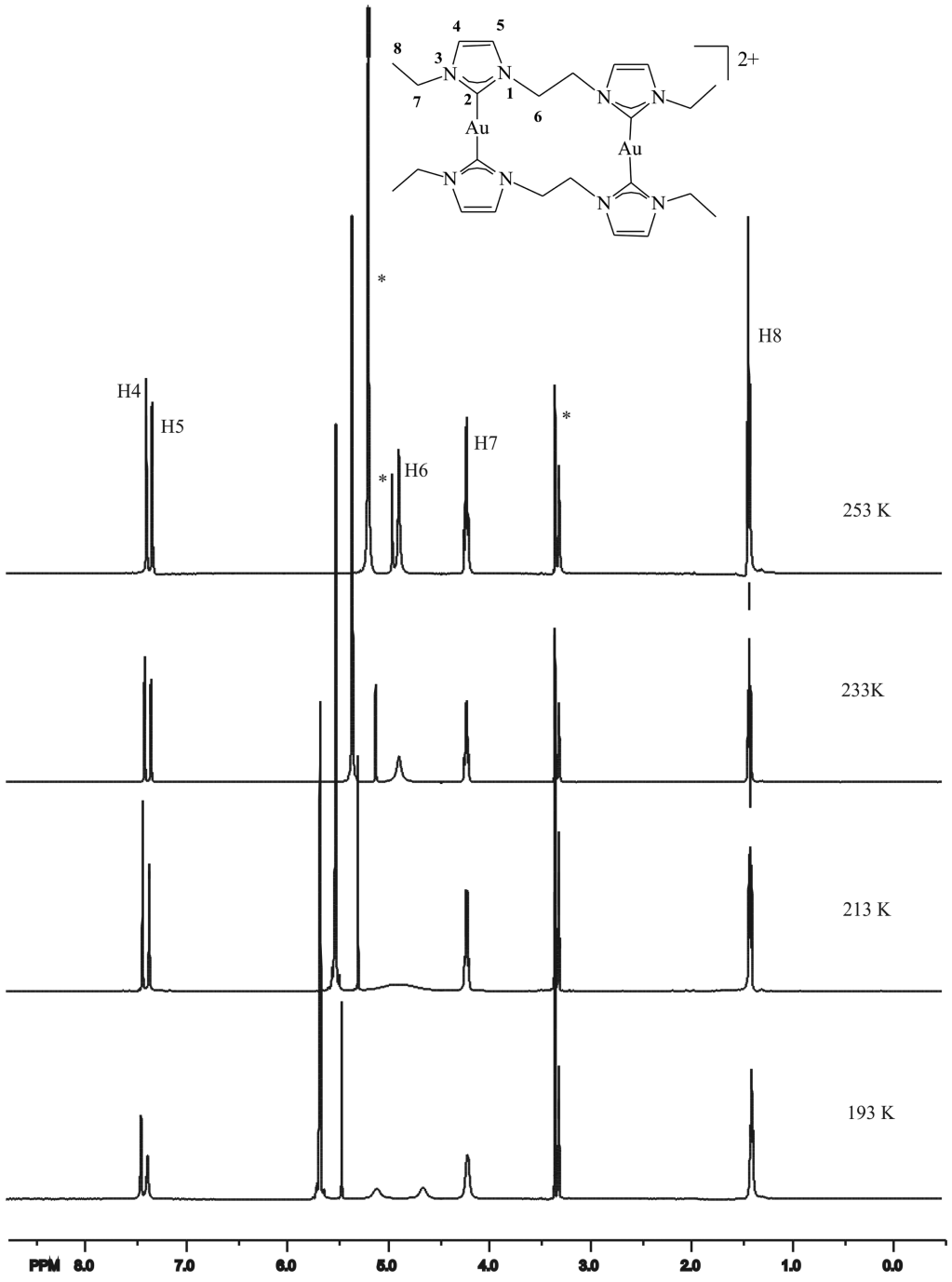

Figure 1. Low-temperature ^{1}H NMR spectra (500.13 MHz, CD_3OD) of **8**. *Partially deuterated and undeuterated methanol and water, respectively.

The protons of the methylene linkers in compounds **7** and **13** are not equivalent and appear as two separated doublets at room temperature.[21a,24,26a] They reversibly disappear/coalesce upon heating to 100−105 °C (Figure S1, Supporting Information) from which the free activation enthalpy at 298 K of $\Delta G_{298}^{\ddagger} = 74 \pm 11$ kJ/mol is extracted from an Eyring plot of exchange rates (Figure S2 and Table S1) obtained by line shape analysis using the program gNMR.[38] A similar behavior has been reported for the methyl-substituted congener and has been attributed to an interconversion of exo and endo hydrogens by a kind of ring inversion (Scheme 2).[21a]

The process is also visible for the methylene protons of the ethyl side groups which are diastereotopic and appear as two multiplets when measured with 500 MHz at room temperature in DMSO-d_6 (Figure S1). Heating the sample (enabling ring inversion) leads to coalescence into the expected quartet signal for equivalent methylene protons. The obtained free activation enthalpy of $\Delta G_{298}^{\ddagger} = 69 \pm 4$ kJ/mol (Figure S2 and Table S1) indeed lies in the error margin of the value obtained using the signal for the bridging methylene groups. An effect of a potentially coordinating anion can be ruled out as similar activation parameters are obtained for the bromide (**7**) and hexafluorophosphate (**13**) salt. Some additional very slight spectral changes reversibly occur upon heating: The signal for the pending methyl protons appears as a triplet which shifts very slightly downfield by 0.05 ppm at higher temperatures. A parallel dynamic behavior is observable for the signal for the imidazolium proton next to the ethyl side chain. It broadens

DOI: 10.1021/ic502751s
Inorg. Chem. 2015, 54, 6100−6111

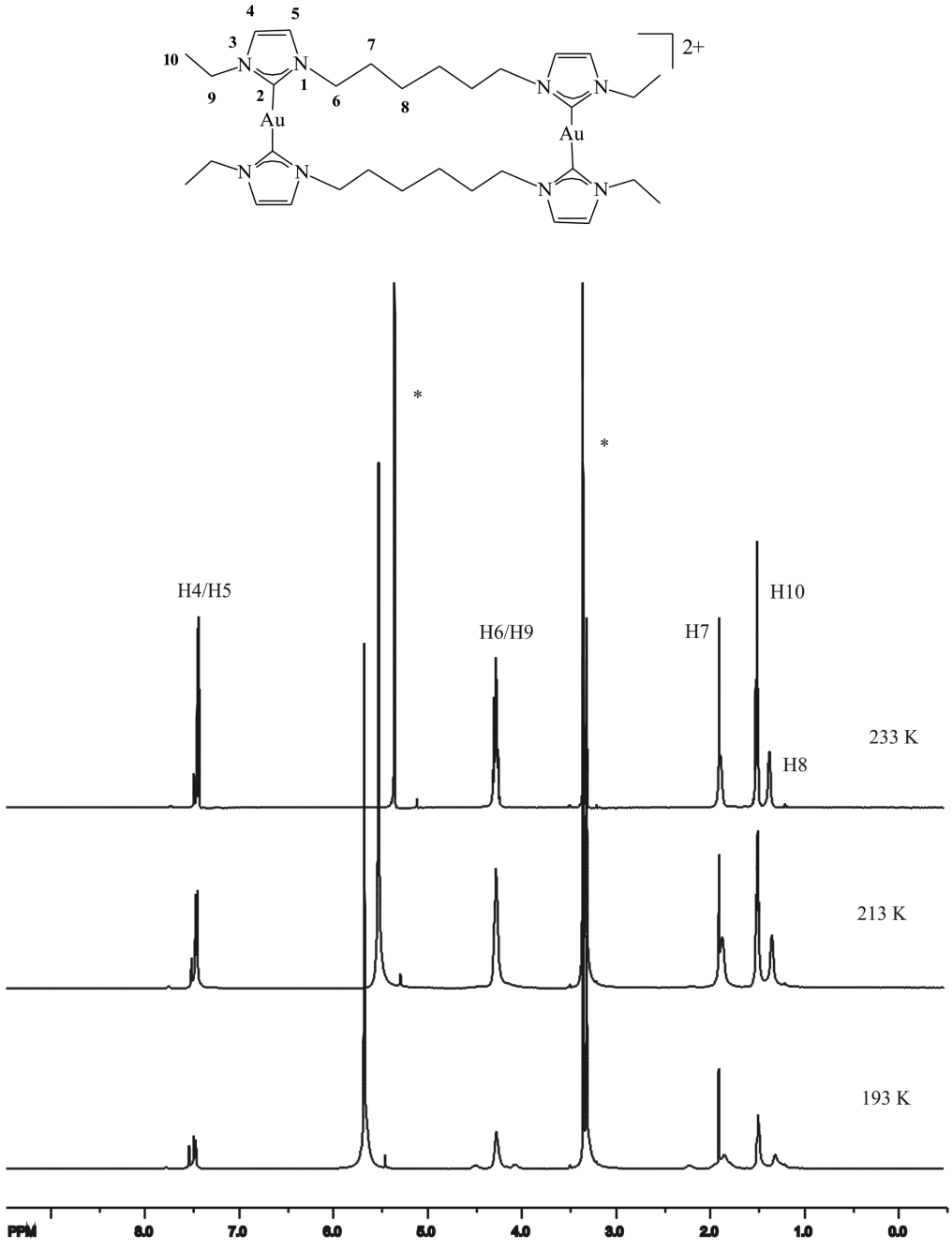

Figure 2. Low-temperature ^{1}H NMR spectra (500.13 MHz, CD_3OD) of **12**. *Partially deuterated and undeuterated methanol and water, respectively.

and resharpens again, similar to the findings reported for the methyl derivative.[21a]

The room temperature ^{1}H NMR spectra for the ethylene-connected macrocycles **8** and **14** show a singlet for eight equivalent linker hydrogens and a well-defined quartet for the side chain methylene groups. Thus, chain elongation expectedly enhances the flexibility of the macrocycles. Lowering the temperature reveals a partial freezing of the conformational flexibility: In the ^{1}H NMR spectra of **8**, a broadening and finally splitting of the linker CH_2 signal into two broad singlets at −80 °C is visible with a coalescence around −60 °C (Figure 1). Line shape analysis (Figure S2 and Table S1) yields $\Delta G_{298}^{\ddagger} = 47 \pm 4$ kJ/mol for the frozen process. It could be interpreted as an inversion of the ethylene-bridged macrocycle equilibrating exo and endo protons in analogy to the behavior of **7** and **13** described above. The smaller ΔH and much lower ΔS value are fully consistent with the enhanced flexibility of the elongated linker. In addition, signal broadening during cooling the sample is visible for the H5 imidazol proton, and, similar to the findings for the smaller macrocycle **7**/**13**, for the CH_2 groups in the ethyl side chains.

The ^{1}H spectra of the macrocycles with C3, C4, and C5 linkers (**9**, **10**, **11**) show broadening of the methylene signals at lower temperatures, but coalescence could not be reached in the temperature range down to −80 °C (Figures S2−S4). The changes in the spectra for **10** are rather subtle, whereas broadening of the H8 signal is clearly visible for compound **9**. For compound **11**, the imidazol protons broaden and shift

DOI: 10.1021/ic502751s
Inorg. Chem. 2015, 54, 6100−6111

Table 1. Selected Structural Data for Complexes 7−18

	n	crystal symmetry	Au−C/ Å	C−Au−C/°	N−C−C−N/°[a]	dihedral angle of NHC planes/°[b,c]	conformation next to NHC	Au·Au/Å intramolecular[d]	Au·Au/Å intermolecular[d]	$\pi\cdot\pi$/Å intermolecular[d]
7	1	$P2_1/n$	2.015(12)	170.0	−4.6	0.8		3.6633(1)	3.57866(16)	3.48279(16)
			2.018(13)	174.5	−1.4	28.1				
			2.026(12)			*109.0*				
			2.031(12)			*107.9*				
8	2	$P2_1/n$	2.018(5)	173.8	−42.8	43.3	gauche	3.3988(1)	7.2397(3)	3.91031(16)
			2.021(5)	177.4	−56.9	55.8				
			2.023(5)			*51.9*				
			2.025(5)			*38.8*				
9	3	*Pmmn*	2.012(5)	178.6	0.0	6.0	trans	6.7918(3)	7.1092(4)	3.6215(3)
						126.3				
10	4	$P\bar{1}$	2.01734(14)	175.7	3.5	3.2	gauche	6.7729(4)	3.69214(15)	3.59182(14)
			2.01675(13)							
12	6	$P\bar{1}$	1.99590(16)	178.8	2.2	6.0	gauche	8.7084(7)	3.8164(3)	3.6865(3)
			2.02309(16)							
13	1	$C2/m$	2.017(5)	172.6	0.0	11.4		3.6475(5)	5.2346(8)	3.6386(5)
			2.022(5)	174.3		14.5				
						106.2				
14	2	$P2_1/c$	2.025(3)	175.3	−49.4	47.0	gauche	3.2328(2)	6.2975(2)	3.49732(15)
			2.027(3)	176.2	−55.5	49.7				
			2.032(3)			*39.1*				
			2.032(3)			*41.9*				
15	3	$P\bar{1}$	2.0069(3)	175.6	1.5 1.6	11.4	trans	6.4190(9)	3.2916(4)	3.5878(4)
			2.0151(3)	176.6		7.9				
			2.0261(3)			*103.4*				
			2.0333(3)			*104.8*				
16	4	$P\bar{1}$	2.057(2)	176.5	2.4	3.3	gauche	6.972(6)	3.5818(25)	3.607(3)
			2.061(2)							
17	5	$C2/c$	2.01847(6)	176.7	2.5	3.7	gauche	4.9425(2)	3.5478(1)	3.74249(12)
			2.02094(6)							
18	6	$P\bar{1}$	2.036(15)	177.3	−7.3	4.4	gauche	8.8268(7)	3.3582(2)	3.5897(2)
			2.046(14)							

[a]Torsion angle between the two NHC rings (EtN−$C_{carbene}$−$C_{carbene}$−NEt) coordinating an Au atom. [b]Dihedral angle of the two NHC planes coordinating an Au atom. [c]Italic: Dihedral angle of the two NHC planes in the linker. [d]The shortest value (NHC plane center to center) is given.

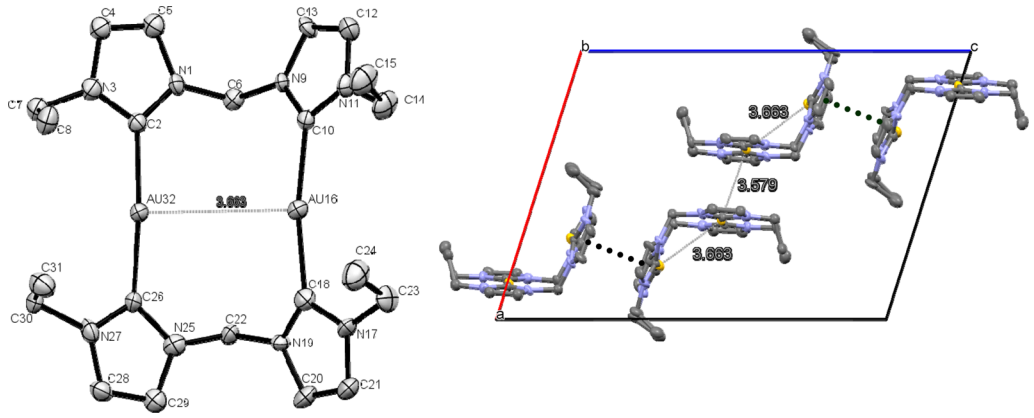

Figure 3. ORTEP drawing (left) and crystal packing (view along b axis, right) of complex **7** (50% probability level for the thermal ellipsoids). Intermolecular $\pi-\pi$ interactions are indicated by dotted lines. Br^- anions, hydrogen atoms, and cocrystallized methanol molecules have been omitted for clarity.

downfield by 0.1 ppm, and the CH_2 and CH_3 signals of the ethyl groups broaden and shift upfield by 0.3 and 0.15 ppm, respectively.

For substance **12** with six methylene units in the linker, sample cooling has a different effect on the ^{1}H NMR spectra (Figure 2). At 193 K, additional broad signals are clearly visible, which we interpret as signs of a starting aggregation inspired by the solid state packing with dominant $\pi-\pi$ interactions arranging the cations in long chains (vide infra).

X-ray Crystal Structures. Single crystals suitable for X-ray diffraction could be obtained by slow diffusion of diethyl ether in a methanol solution (**7**−**10**, **12**) or an acetonitrile solution (**13**−**18**). Thus, 11 out of 12 new complexes were structurally characterized. Selected structural data are summarized in Table

DOI: 10.1021/ic502751s
Inorg. Chem. 2015, 54, 6100−6111

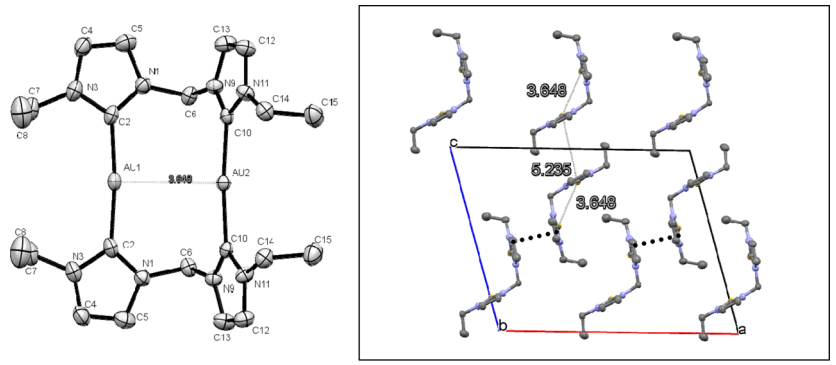

Figure 4. ORTEP drawing (left) and crystal packing (view along *b* axis, right) of complex **13** (50% probability level for the thermal ellipsoids). Intermolecular $\pi-\pi$ interactions are indicated by dotted lines. PF_6^- anions and hydrogen atoms have been omitted for clarity.

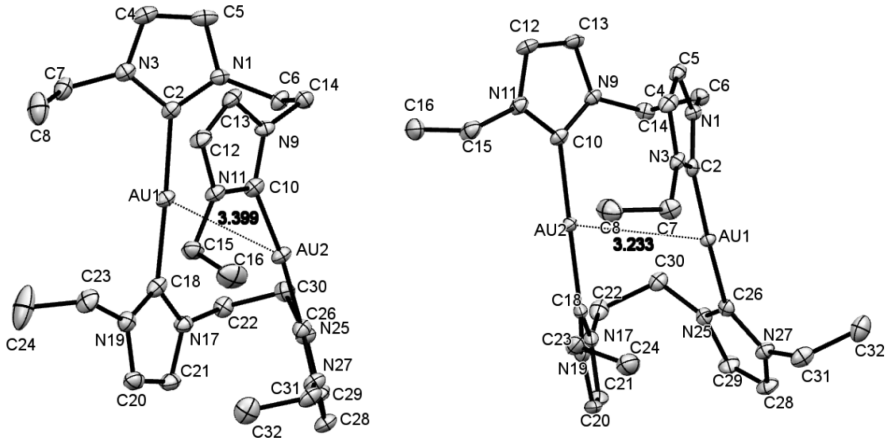

Figure 5. ORTEP drawing of complex **8** (left) and **14** (right) (50% probability level for the thermal ellipsoids). Anions (Br^- and PF_6^-, respectively), hydrogen atoms and cocrystallized water and methanol (for **8**) have been omitted for clarity.

1. All compounds consist of dicationic dinuclear complexes $Au_2L_2^{2+}$ with bridging dicarbene ligands L. The basic structural parameters fit the expectations: The gold atoms are two-coordinated with C−Au−C angles close to linearity and mean C−Au bond lengths of 2.02 Å typical for gold(I) NHC compounds.[1] Owing to the almost linear C−Au−C axis, the torsion angles can be measured between N−C−C−N of the two ligands coordinating a gold atom to describe the position of these ligands. For all cations studied here except for the ones with ethylene linkers **8** and **14**, the torsion angle is close to zero, and the NHC planes on opposite sides of the gold are coplanar. Each cation is accompanied by two bromide or hexafluorophosphate anions, respectively. In all cases, the complexes are arranged in layers consisting of organic ligands on the one hand and gold atoms with anions on the other. NHC ligands of neighbored complexes are interconnected by $\pi-\pi$ interactions. Further, all solid state structures except for **9** reveal a relatively short Au−Au distance, either intra- or intermolecularly; in one case (**7**) even both is realized. The space groups and crystal packing of the two complexes with the same cation typically differ due to the significant difference in size of the two anion types. However, the influence of the counterion on the conformation of the cation is unexpectedly small (Figures 3−10 and S7−S18, Table 1) compared to examples in the literature.[19,26]

One of the more obvious conformational differences is observed for the smallest cation bearing only methylene linkers. Here, all ethyl side chains point inward for the bromide salt **7** (Figure 3), but show an in/out conformation for **13** with PF_6^- (Figure 4). In both cases, the ethyl side groups of the two NHC rings coordinating an Au atom come rather close (Figure S6). The angles of the NHC substituents at the methylene group are identical (111.8° and 111.1°, respectively), and the intramolecular Au−Au distance (3.663 Å vs 3.648 Å) is only 0.016 Å shorter for **13**. The crystal structure of both **7** and **13** consists of pairs of macrocycles with parallel arrangement of a whole NHC-Au-NHC unit. The dimers of macrocycles are further connected by head-to-tail $\pi-\pi$ interactions with neighboring NHC units (Figures S7 and S8). The intermolecular distance between the gold atoms of a dimer of macrocycles is much shorter in **7** (3.579 Å) than in **13** (5.235 Å) due to the different orientation of the ethyl side chains.

A similar complex published by Barnard et al. has a methyl side group and I^- as counterion.[21a] The shape of the cation is comparable to **7** and **13**, but the intramolecular Au−Au distance is shorter (3.5425(6) Å). Further, Hemmert and co-workers structurally characterized two methylene-bridged gold-NHC complexes with alcohol- or carboxylate-functionalized side chains (Au−Au 3.514 and 3.589 Å, respectively).[24] An even shorter distance (3.3610(7) Å) could be realized by Fränkel et al.[20a] in a neutral complex containing a BH_2-unit instead of a methylene linker and by the group of Hahn via incorporation into a large macrocycle (3.0737(3) Å).[29c]

C2-linked complexes **8** and **14** both crystallize in monoclinic space groups as well (**8**: $P2_1/n$, **14**: $P2_1/c$). The overall conformation of the dicationic macrocycle is unusual, but rather similar for both anion types (Figure 5) apart from the relative position of the ethyl side groups. A backfolded twisted

DOI: 10.1021/ic502751s
Inorg. Chem. 2015, 54, 6100−6111

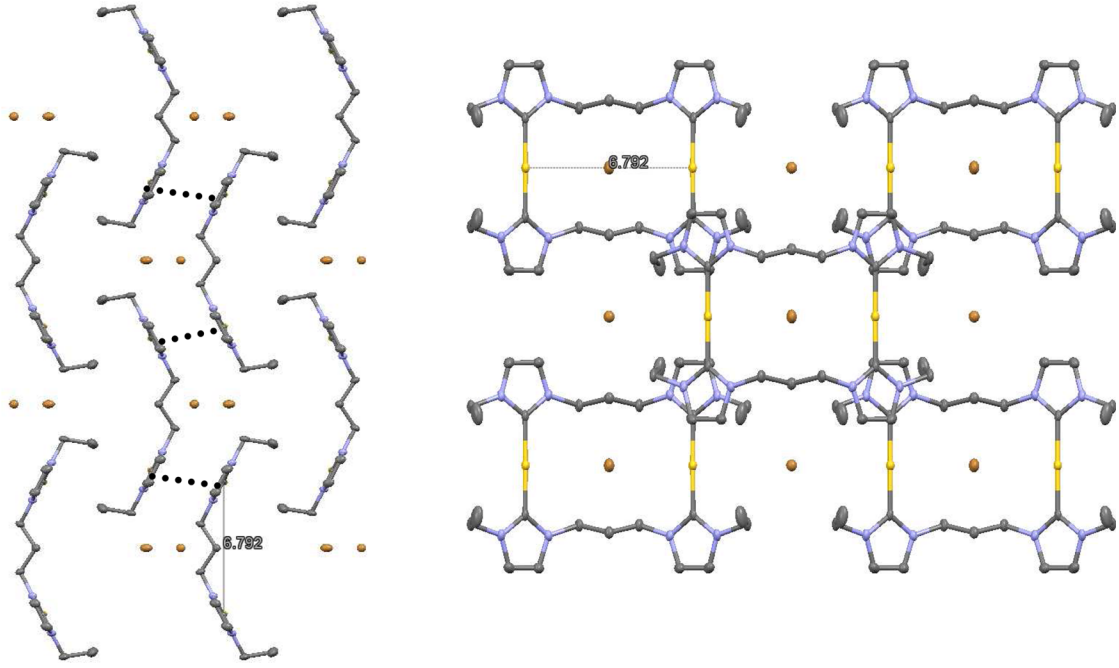

Figure 6. Crystal packing of complex **9** (view along *b* (left) and *c* (right) axes, 50% probability level for the thermal ellipsoids). The macrocycles form double-layers connected by intermolecular $\pi-\pi$ interactions indicated by dotted lines. Hydrogen atoms have been omitted for clarity.

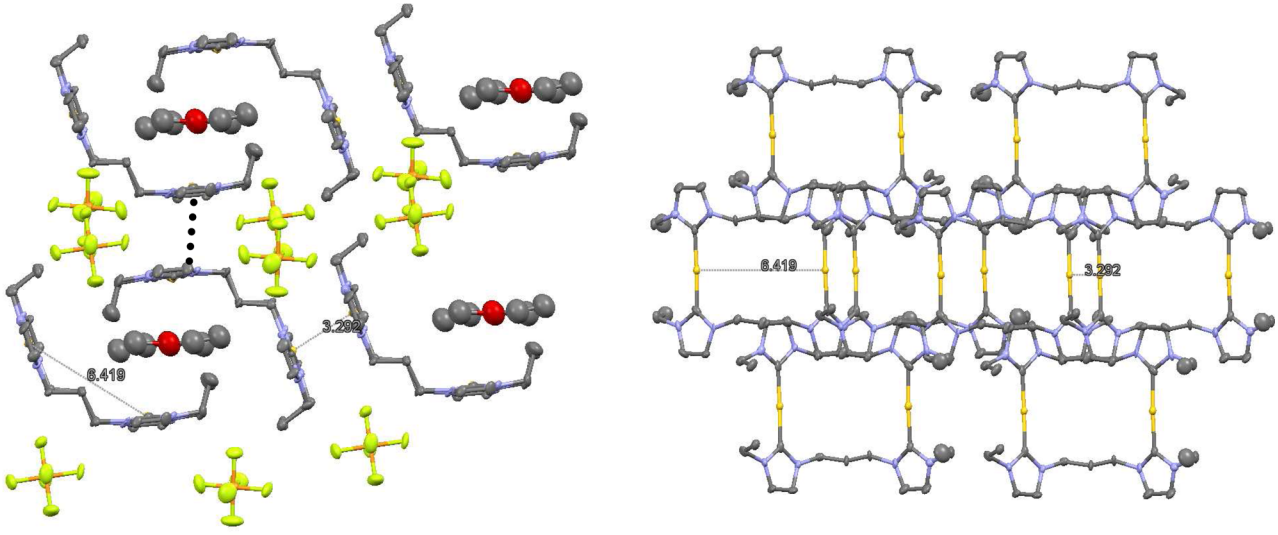

Figure 7. Two views of the crystal packing of complex **15** (50% probability level for the thermal ellipsoids). Au–Au bonded dimers of macrocycles are connected by intermolecular $\pi-\pi$ interactions indicated by dotted lines. Hydrogen atoms and in the right view also PF_6^- anions and cocrystallized Et_2O and have been omitted for clarity.

geometry with gauche conformation in the ethylene linkers realizes a short intramolecular Au–Au distance (**8**: 3.3988(1) Å, **14**: 3.2328(2) Å). The Au–Au bond is significantly (Δd = 0.167 Å) shorter for the bigger hexafluorophosphate. This cation is the only one of the whole series for which the two NHC planes bound to a gold atom are not coplanar, but twisted by approximately 50°—probably to avoid steric repulsion of the ethylene linkers while retaining the short Au–Au distance. The conformational folding of the dication in **8** is so compact and twisted that a close arrangement with neighboring macrocycles is restricted to a single $\pi-\pi$ interaction per molecule (Figure S9).

The only published ethylene-linked NHC-Au complex structurally characterized by X-ray bears a bulky alcohol-functionalized side group and PF_6^- anions.[24b] Its conformation is backfolded with 50° twisted NHC planes and an intramolecular Au–Au bond in the range of 3.3 Å. It strongly resembles the conformations of the ethyl derivates described here. The fact that all side chains point to the same side of the molecule thus is not (only) due to hydrogen bonds between OH groups because a similar conformation is retained with simple ethyl groups as well. Considering the absence of strong intra- or intermolecular $\pi-\pi$ interactions, the observed backfolded conformation should have an attractive aurophilic origin even though the two gold atoms are cationic.

Both dications **9** and **15** with C3-linked NHC ligands show an open, W-like conformation with an all-*trans* propylene linker (Figures 6 and 7). The intramolecular Au–Au distance is very

DOI: 10.1021/ic502751s
Inorg. Chem. 2015, 54, 6100–6111

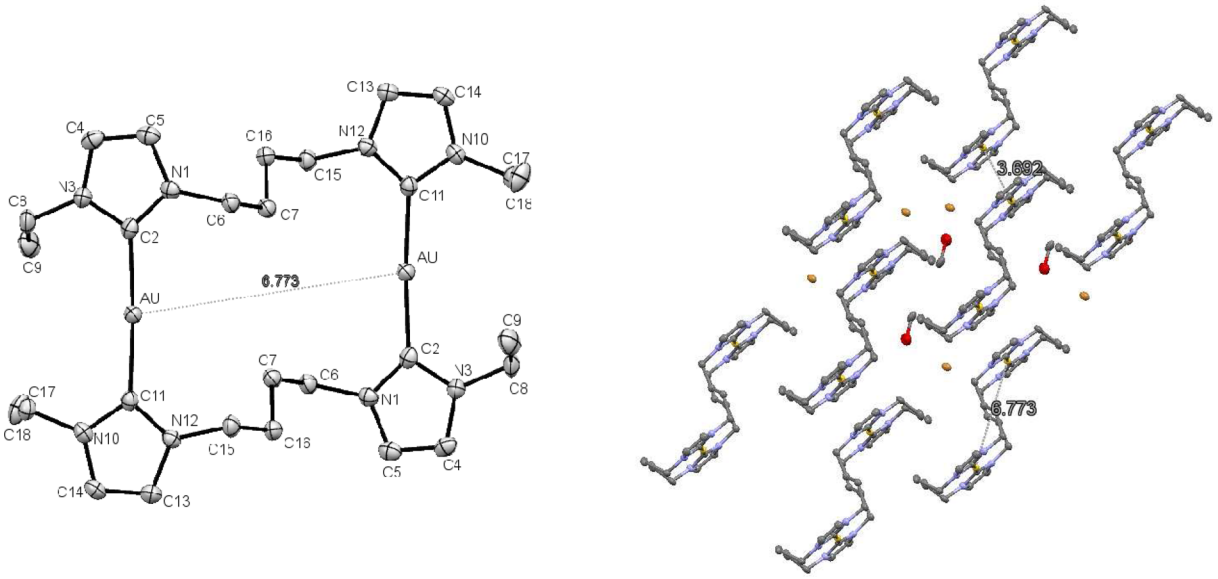

Figure 8. ORTEP drawing and crystal packing of complex **10** (50% probability level for the thermal ellipsoids). Hydrogen atoms have been omitted for clarity.

long for both structures, but in the Br^- case even 0.373 Å longer than with PF_6^-. This is the result of a flattened conformation as the dihedral angle of 103−105° between the two NHC planes of a ligand in the PF_6^- structure **15** is widened to 126° when crystallized as the bromide salt **9** (Figure S10). The reason probably is a packing effect: The crystal packing of **15** closely resembles the one of methylene-linked **7**. Dimers of macrocycles are formed by a short intermolecular Au−Au distance of 3.292 Å, and these dimers are connected by $\pi-\pi$ interactions (Figure S11). In contrast, the bromide derivative **9** appears in extended $\pi-\pi$ bound double-layers (Figure 6, left), which should be easier to form with flattened macrocycles. It is the only structure of our series that does not show any kind of intra- or intermolecular Au−Au interaction.

Baron et al. reported the crystal structure of a related propylene bridged Au(I) NHC complex with methyl side chains and PF_6^- as counterion in 2012.[26a] Unlike the situation shown here, the alkyl chains fold in two gauche conformations resulting in a U-shaped macrocycle with parallel NHC-Au-NHC subunits and a short intramolecular gold(I)−gold(I) distance of 3.272 Å. Gil-Rubio et al. crystallized the same cation with triflate anions in 2013.[19] This time a helical conformation with orthogonal NHC-Au-NHC bonds and a very small Au−Au-distance of 3.032 Å is realized. In both structures, the backfolded macrocycles form C3- and C2-symmetric columnar aggregates, respectively, with intermolecular Au−Au and $\pi-\pi$ interactions of about d = 3.7 Å. In contrast, the third literature-known structurally characterized propylene-bridged complex of this type crystallizes in an open conformation and a double-layer packing without Au−Au interactions,[24a] which strongly resembles the findings reported above for the ethyl derivative **6**. It stems from the Hemmert group and possesses PF_6^- anions and bulky side groups with hydroxyl functions. Thus, counterion and the type of side group have an extreme effect on the molecular conformation of propylene-linked dinuclear NHC complexes of gold(I). In particular, the steric increase from methyl to ethyl is sufficient to open the conformation and suppress the formation of an intramolecular Au−Au bond.

Complexes **10** and **16** with the C4-linker crystallize in the triclinic space group $P\bar{1}$. Both the cation conformations and crystal packing are rather similar (Figures 8, S12−S14). The cations show an open S-arrangement with a very long intramolecular Au−Au distance and gauche conformations in the linker enabling coplanarity for all NHC rings. Intermolecular $\pi-\pi$ and Au−Au interactions connect the molecules into chains. It is very plausible that these packing effects are the dominating cause for the observed conformation.

Although purification by crystallization was successful for the bromide salt **11**, the resulting crystals were not suitable for X-ray diffraction measurements. Yet, the PF_6^- version **17** gave good crystals in the monoclinic space group $C2/c$. The conformation of the cation is rather unusual compared to the other complexes of this series (Figure 9), but it bears some resemblance to the C3-triflate structure reported by Gil-Rubio et al. briefly mentioned above.[19] The two C−Au−C axes are not parallel, but twisted by approximately 60° resulting in a compact helical cation with a relatively long intramolecular

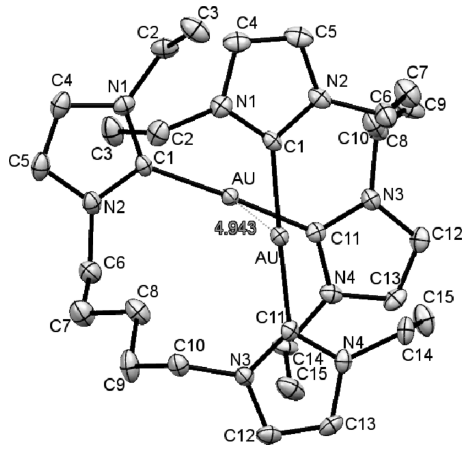

Figure 9. ORTEP drawing of complex **17** (50% probability level for the thermal ellipsoids). PF_6^- anions and hydrogen atoms have been omitted for clarity.

DOI: 10.1021/ic502751s
Inorg. Chem. 2015, 54, 6100−6111

Au−Au distance of 4.9425(2) Å. All NHC planes are coplanar with the ethyl side chains facing inside (Figure S15). Thus, columnar chains are formed by $\pi-\pi$ stacking and shorter intermolecular gold−gold distances of 3.548 Å. Even though the molecular conformation is rather different from those observed for the C4 of C6 derivates, the similarities in the NHC-dominated packing motifs are obvious (Figures S12 and S15).

There is only one report of dimeric gold-NHC complexes with a linker of similar length in the literature so far.[22] A species with an oxygen atom in the central position of the linker, naphthalene side groups, and PF_6^- anions has been structurally characterized. The conformation of this dication resembles the one of **17** in that it is helically twisted with a torsion angle of 68°. The intramolecular Au−Au distance (3.506 Å) is much shorter, whereas there are no intermolecular Au−Au interactions because the large aromatic side groups are turned outward and dominate the packing.

Similar to the findings for the C4-analogues **10** and **16**, the cations in the C6-linked complexes **12** and **18** retain an open S-shaped conformation (Figures 10 and S16−S18) that allows

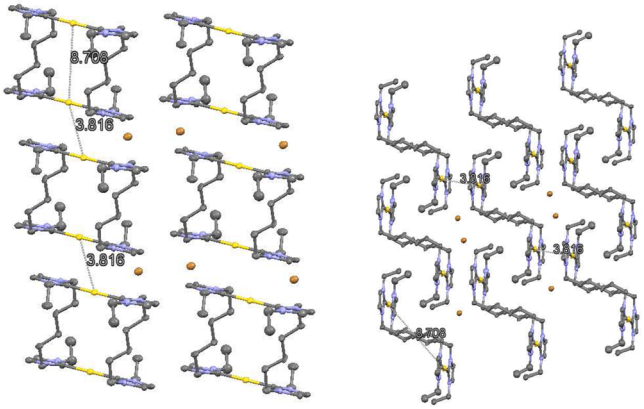

Figure 10. Two views of the crystal packing of complex **12** (50% probability level for the thermal ellipsoids). Hydrogen atoms have been omitted for clarity.

coplanarity for all NHC rings (Figures 10 and S18). The cations again are connected into chains by intermolecular Au−Au distances of 3.8164 Å (**12**) and 3.3582 Å (**18**). The longer distance in the bromide complex is due to a larger shift in the $\pi-\pi$ stacking; the intermolecular distance between the NHC planes is rather similar for both compounds. This is another indication for the dominance of $\pi-\pi$ interactions in the crystal packing. The alkyl linkers adopt two gauche conformations next to the NHC rings necessary to enable π-stacking. In addition, the typical all-*trans* parallel alignment expected for alkyl chain crystals is observed for the inner methylene groups.

Optical Spectroscopy. UV/vis absorption spectra of the complexes **7** − **12** in solution or solid state show absorption maxima around 260 nm (Figure S19) tentatively assigned to intraligand transitions.[34b] Excitation in that band leads to emission spectra that strongly vary depending on the linker chain length (Figure 11). A priori, one might expect decreasing fluorescence with increasing chain length due to an enhanced flexibility and thus vibrational relaxation of the excited state. This is indeed the case for the moderate emission of the imidazolium ligand precursors which is most intense for the smallest, methylene-linked species. Fluorescence in the corresponding complexes **7** and **13** however is quenched, which could be the result of a metal-mediated deactivation process. In contrast, the complexes with linker length $n = 2$ and $n = 3$ show a completely different behavior, i.e., a strong luminescence at 365 and 372 nm, respectively, which significantly weakens for longer linkers. This nicely correlates with the observation of conformations with short intramolecular Au−Au distances only for linker chain lengths of $n = 2$ and $n = 3$.

Theory. After observing experimentally how the delicate balance of interactions within these gold complexes influences the intramolecular conformation and intermolecular packing structure, we decided to use quantum chemical calculations to study the presence of the aurophilic interplay, which is perhaps the most characteristic structural factor of the hereby investigated complexes. Theory has been shown to be a fruitful tool in describing and understanding gold complexes in general and gold−gold interactions in particular.[31,39] In this respect, the several successful applications of DFT for such problems[31b] or even to gold clusters may be mentioned.[40]

The unit cells of **7**, **8**, and **13** were optimized by various methods in the gas phase, and the Au−Au distances were inspected together with the electronic structure in terms of shared electron numbers (SEN). The results are shown in Table 2. The Au−Au distances in the optimized structures vary greatly depending on the theoretical method applied (up to even 0.3 Å), which is in agreement with the expected high flexibility of these molecules. Generally, the optimization with the larger basis set (def2-TZVPP) resulted in smaller gold−gold distances. The shortest distances were obtained if the TPSS meta-GGA functional was applied, while the PBE functional gave only slightly longer ones. The structures with the BP86 and B97-D functionals showed significantly longer gold−gold distances, and the longest were in all cases those yielded by BLYP.

Apparently, in the case of **7** and **13** the calculations indicate shorter, while in case of **8** longer Au−Au distances than those obtained from the X-ray measurements. The presence of some discrepancy is in fact not surprising, since the crystal packing effects are not included in the present gas phase calculations. The intermolecular interactions are obviously strongly influencing the experimental solid state structures; for example, comparing the intra- and intermolecular gold−gold distances for **7**, it is apparent that the intermolecular aurophilic interaction might be even stronger than the intramolecular one, similarly to structures **10**, **12**, **15**−**18** (Table 1). In addition, the conformation of the ring due to the intermolecular $\pi-\pi$ interactions can alter the orientation of the gold atoms with respect to each other. The intermolecular effects will be explored in a follow-up study, where the competitive or cooperative nature of these interactions will be explored in more detail. Despite the expected discrepancies between the gas phase calculations and the solid state experimental structures, it is very useful to inspect the present results for the gas phase systems, since the interactions that govern the structure in the gas phase are expectedly also present in the crystal.

The Au−Au distances are similar in **7** and **13**, and—except for the data obtained by PBE—tend to be shorter for **7** as in the experimental data. In the case of **8** the calculated distance is significantly larger than for the other two species, while the experimental value is shorter (Table 1). These peculiar results, on one hand, clearly show that the length of the linking side

DOI: 10.1021/ic502751s
Inorg. Chem. 2015, 54, 6100−6111

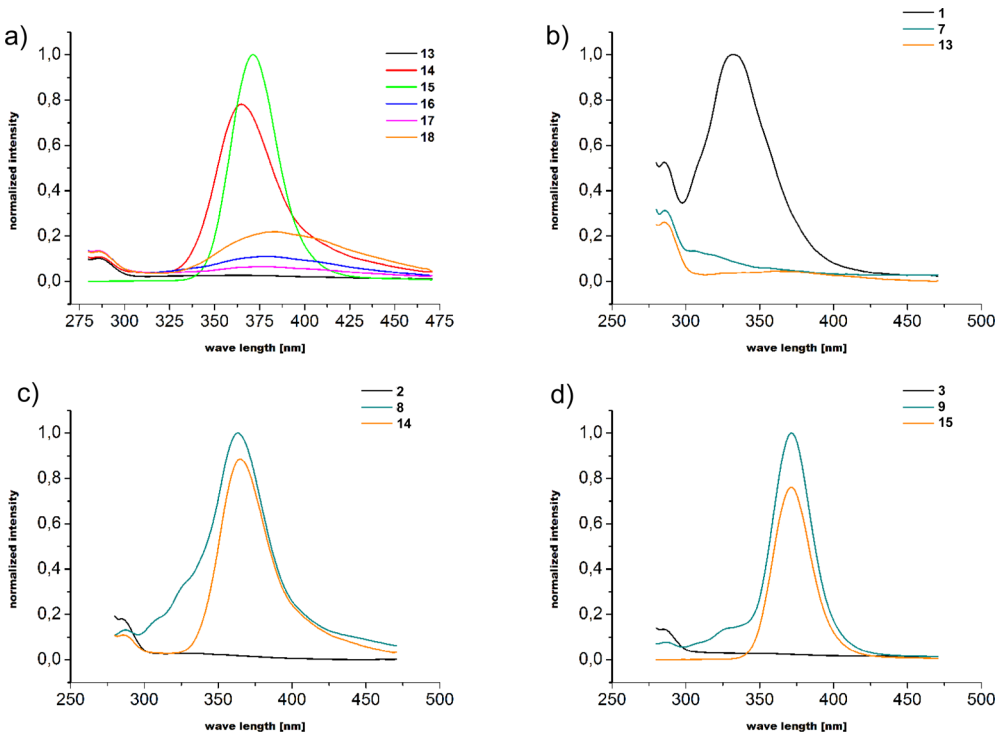

Figure 11. Fluorescence spectra measured in acetonitrile at room temperature after excitation at 265 nm: (a) hexafluorophosphate complexes **13**–**18**, (b–d) comparison of imidazolium ligand precursor, bromide and hexafluorophosphate complex for linker lengths n = 1–3.

Table 2. Gold–Gold Distances in the Optimized Structures of 7, 8, and 13, Together with the Corresponding Shared Electron Number (SEN) Data[a]

	7		8		13		water dimer
	d_{Au-Au}/Å	SEN/a.u.	d_{Au-Au}/Å	SEN/a.u.	d_{Au-Au}/Å	SEN/a.u.	SEN/a.u.
RI-BP-D3/def2-SV(P)	3.384	0.153	3.569	0.010	3.472	0.158	
RI-BP-D3/def2-TZVPP	3.302	0.028	3.582	0.009	3.356	0.017	0.040
RI-BP-D3/def2-QZVPP// RI-BP-D3/def2-TZVPP	3.302	0.020	3.582	0.015	3.356	0.025	0.038
RI-B97-D3/def2-SV(P)	3.429	0.132	3.577	0.010	3.480	0.012	
RI-B97-D3/def2-TZVPP	3.406	0.021	3.569	0.010	3.466	0.014	0.031
RI-B97-D3/def2-QZVPP// RI-B97-D3/def2-TZVPP	3.406	0.015	3.569	0.013	3.466	0.020	0.029
RI-BLYP-D3/def2-SV(P)	3.499	0.127	3.655	0.008	3.552	0.113	
RI-BLYP-D3/def2-TZVPP	3.477	0.019	3.681	0.008	3.533	0.014	0.036
RI-BLYP-D3/def2-QZVPP// RI-BLYP-D3/def2-TZVPP	3.477	0.016	3.681	0.013	3.533	0.020	0.033
RI-PBE-D3/def2-SV(P)	3.389	0.148	3.549	0.011	3.334	0.533	
RI-PBE-D3/def2-TZVPP	3.296	0.031	3.550	0.010	3.324	0.019	0.043
RI-PBE-D3/def2-QZVPP// RI-PBE-D3/def2-TZVPP	3.296	0.022	3.550	0.013	3.324	0.025	0.037
RI-TPSS-D3/def2-SV(P)	3.256	0.179	3.465	0.014	3.320	0.291	
RI-TPSS-D3/def2-TZVPP	3.191	0.039	3.416	0.016	3.265	0.023	0.041
RI-TPSS-D3/def2-QZVPP// RI-TPSS-D3/def2-TZVPP	3.191	0.028	3.416	0.015	3.265	0.028	0.038

[a]For comparison, data for the population analyses of the hydrogen bond in a water dimer are also presented.

chain is clearly of great importance, while on the other hand they show that intermolecular effects play a really dominating role. Considering the trends mentioned above, one might speculate that in the case of **7** and **13** the intermolecular effects *decrease*, while in the case of **8** they *increase* the aurophilic interplay.

The shared electron number data show that there is a notable interaction between the orbitals of the two gold atoms for all structures and by all methods, although its strength varies largely by the system and the applied method. In the case of **7** and **13**, the smallest basis set (def2-SV(P)) gave erroneously high shared electron numbers despite the significantly larger distances, compared to the two larger basis sets. The increase from triple-ζ to quadruple-ζ basis set in the electronic structure method, however, results in a much smaller change. In accordance with the calculated distances, **8** showed the weakest orbital–orbital interactions among the three species. Interestingly, however, despite the slightly longer Au–Au distances, the SEN tends to be somewhat higher for **13** than for **7** according to the data obtained with the largest basis set. Consideration of only the distances thus is not a sufficient criterion for describing the extent of aurophilicity. This is especially the case if we compare the SEN data to that obtained for a water dimer (Table 2), which indicates that the binding aurophilic

DOI: 10.1021/ic502751s
Inorg. Chem. 2015, 54, 6100–6111

interactions in the present complexes are 50−95% of the binding hydrogen bond between two water molecules, depending on the complex and on the method as well.

Although our present gas phase data already show the presence of intramolecular aurophilic interactions, we are planning to continue with a systematic joint experimental−theoretical study to explore the interactions within these complexes in a detailed quantitative fashion.

CONCLUSION

We present a systematic series of new dinuclear Au(I) complexes with N-heterocyclic carbene ligands designed as an experimental basis for a deeper understanding of the subtle interplay of weak noncovalent interactions and their effect on molecular conformation and aggregation. In particular, the role of aurophilicity vs π-stacking is addressed, as well as the role of alkyl chain length.

In the smallest case with only a methylene group connecting the NHC ligands, the system is so stiff that a change in ring conformation can be observed by NMR in solution. In contrast, the longer chain lengths from C4 onward are flexible enough to allow coplanarity for all NHC planes. Thus, $\pi-\pi$ stacking rather than aurophilicity seems to dominate their conformations observed in the crystalline state. Additional alkyl chain aggregation is visible for the C4-linker and much more clearly for the C6 case. Even−odd alternation is manifested by the similarity of the C4 and C6 variants, whereas the C5 conformation resembles one conformation observed for a C3 derivate.

The intermediate cases with ethylene and propylene bridges are most interesting. We find backfolded conformations with an intramolecular aurophilic bond for both ethylene-bridged complexes; $\pi-\pi$ interactions do not seem to play a major role there. For related propylene-bridged macrocycles, extremely high fluorescence quantum yields have been reported and correlated with intramolecular Au−Au interactions.[26a] A variety of conformations have been observed depending on counterion and peripheral N-substituent:[19,24a,26a] Two different backfolded examples with methyl side groups oppose a hydroxyl-substituted version with an open outstretched ring. Our ethyl results now show that hydrogen bonds are not necessary for the conformational change. Already the small steric increase of elongating the peripheral methyl into ethyl groups is sufficient to destabilize the backfolding and invoke a preference for an open conformation that maximizes inter- rather than intramolecular attractions.

We plan to study the UV/vis and fluorescence spectroscopy of the presented complexes and their dependence on the actual conformation in more detail. We further work on a extended quantum-chemical study targeting the interplay of $\pi-\pi$ and aurophilic interactions.

EXPERIMENTAL SECTION

General Synthesis of NHC Precursors 1−6. The corresponding alkyldibromide (5 mmol) and N-ethylimidazole (1 mL, 10.4 mmol) were dissolved in dry toluene (15 mL) and stirred for 1−3 days at 110 °C. After cooling to room temperature the white precipitate was filtered, washed with dry toluene/diethyl ether, and dried in vacuo.

Synthesis of (NHC)Au(I)-bromide Complexes 7−12. The corresponding NHC precursor (0.3 mmol) and $Au(SMe_2)Cl$ (88.37 mg, 0.3 mmol) were dissolved in dry DMF (7 mL). To maintain a clear solution, the mixture was heated to 100 °C if applicable. NaOAc (62.27 mg, 0.75 mmol) was added and the solution was stirred for 2−3 h. After cooling to room temperature, diethyl ether (15 mL) was added to precipitate the corresponding complex. The white powder was filtered, washed with diethyl ether, and dried in vacuo. The complexes were purified by crystallization (slow diffusion of diethyl ether into a solution in methanol).

Synthesis of (NHC)Au(I) Hexafluorophosphate Complexes 13−18. The corresponding bromide complex was dissolved in methanol. A solution of KPF_6 in water was added to precipitate the corresponding complex. The white powder was filtered, washed with water and methanol, and dried in vacuo. The complexes were purified by crystallization (slow diffusion of diethyl ether into a solution in acetonitrile).

Theory. For the quantum chemical calculations, the Turbomole 6.4 program package was used.[41] For the optimization of the structures, the BP86,[42] B97-D,[43] BLYP,[42a,b,44] PBE,[42a,b,45] and TPSS[42a,b,46] functionals were applied together with the D3 dispersion correction,[47] and the def2-SV(P),[48] and def2-TZVPP[48] basis sets. On the gold atoms, def2-ecp pseudopotentials[49] were applied, containing a scalar correction to relativistic effects. During the geometry optimizations the SCF convergence was set to 10^{-8} a.u., while the maximum gradient was converged below 10^{-4} a.u. To check if the shared electron numbers are reasonable in the case of the def2-TZVPP basis sets, these calculations on the def2-TZVPP structures have been performed with the def2-QZVPP basis set[48] as well.

ASSOCIATED CONTENT

Supporting Information

Additional figures, experimental details, spectroscopic data, crystallographic information. The Supporting Information is available free of charge on the ACS Publications website at DOI: 10.1021/ic502751s.

AUTHOR INFORMATION

Corresponding Author

*E-mail: Marianne.Engeser@uni-bonn.de.

Present Address

#(C.M.-T.) Institute of Inorganic and Analytical Chemistry, Johannes Gutenberg-University, 55122 Mainz, Germany.

Notes

The authors declare no competing financial interest.

ACKNOWLEDGMENTS

Financial support by the Jürgen Manchot Stiftung and the Deutsche Forschungsgemeinschaft is acknowledged. We thank Charlotte Rödde for X-ray structure determinations, Volker Dittrich for solid state UV absorption spectra and appreciate very helpful discussions with Dr. Senada Nozinovic.

REFERENCES

(1) (a) Lin, I. J. B.; Vasam, C. S. *Can. J. Chem.* **2005**, *83*, 812−825. (b) Lin, J. C. Y.; Huang, R. T. W.; Lee, C. S.; Bhattacharyya, A.; Hwang, W. S.; Lin, I. J. B. *Chem. Rev.* **2009**, *109*, 3561−3598.

(2) (a) Hashmi, A. S. K.; Hutchings, G. J. *Angew. Chem., Int. Ed.* **2006**, *45*, 7896−7936. (b) Marion, N.; Nolan, S. P. *Chem. Soc. Rev.* **2008**, *37*, 1776−1782. (c) Nolan, S. P. *Acc. Chem. Res.* **2011**, *44*, 91−100.

(3) *Chem. Soc. Rev.* **2008**, *37*, Issue 9: Chemistry, Materials and Catalysis of Gold.

(4) Lee, K. M.; Lee, C. K.; Lin, I. J. B. 1997, *36*, 1850−1852.

(5) *Coord. Chem. Rev.* **2009**, *253*, Issue 11−12: Bioinorganic and Biomedical Chemistry of Gold.

(6) Mohr, F., Ed. *Gold Chemistry. Applications and Future Directions in the Life Sciences*; Wiley-VCH: Weinheim, 2009.

(7) (a) Barnard, P. J.; Berners-Price, S. J. *Coord. Chem. Rev.* **2007**, *251*, 1889−1902. (b) Hindi, K. M.; Panzner, M. J.; Tessier, C. A.; Cannon, C. L.; Youngs, W. J. *Chem. Rev.* **2009**, *109*, 3859−3884.

DOI: 10.1021/ic502751s
Inorg. Chem. 2015, 54, 6100−6111

(8) (a) Wang, H. M. J.; Lin, I. J. B. *Organometallics* **1998**, *17*, 972−975. (b) Wang, H. M. J.; Chen, C. Y. L.; Lin, I. J. B. *Organometallics* **1999**, *18*, 1216−1223.
(9) Jahnke, M. C.; Pape, T.; Hahn, F. E. *Z. Naturforsch.* **2013**, *68b*, 467−473.
(10) de Frémont, P.; Scott, N. M.; Stevens, E. D.; Nolan, S. P. *Organometallics* **2005**, *24*, 2411−2418.
(11) Messori, L.; Marchetti, L.; Massai, L.; Scaletti, F.; Guerri, A.; Landini, I.; Nobili, S.; Perrone, G.; Mini, E.; Leoni, P.; Pasquali, M.; Gabbiani, C. *Inorg. Chem.* **2014**, *53*, 2396−2403.
(12) Bonati, F.; Burini, A.; Pietroni, B. R.; Bovio, B. *J. Organomet. Chem.* **1989**, *375*, 147−160.
(13) (a) Raubenheimer, H. G.; Lindeque, L.; Cronje, S. *J. Organomet. Chem.* **1996**, *511*, 177−184. (b) Raubenheimer, H. G.; Olivier, P. J.; Lindeque, L.; Desmet, M.; Hrusak, J.; Kruger, G. J. *J. Organomet. Chem.* **1997**, *544*, 91−100. (c) Horvath, U. E. I.; Bentivoglio, G.; Hummel, M.; Schottenberger, H.; Wurst, K.; Nell, M. J.; van Rensburg, C. E. J.; Cronje, S.; Raubenheimer, H. G. *New. J. Chem.* **2008**, *32*, 533−539.
(14) (a) Baker, M. V.; Barnard, P. J.; Berners-Price, S. J.; Brayshaw, S. K.; Hickey, J. L.; Skelton, B. W.; White, A. H. *Dalton Trans.* **2006**, 3708−3715. (b) Hickey, J. L.; Ruhayel, R. A.; Barnard, P. J.; Baker, M. V.; Berners-Price, S. J.; Filipovska, A. *J. Am. Chem. Soc.* **2008**, *130*, 12570−12571.
(15) Samantaray, M. K.; Pang, K.; Shaikh, M. M.; Ghosh, P. *Inorg. Chem.* **2008**, *47*, 4153−4165.
(16) Kunz, P. C.; Wetzel, C.; Kögel, S.; Kassack, M. U.; Spingler, B. *Dalton Trans.* **2011**, *40*, 35−37.
(17) Hemmert, C.; Fabié, A.; Fabre, A.; Benoit-Vical, F.; Gornitzka, H. *Eur. J. Med. Chem.* **2013**, *60*, 64−75.
(18) Wang, J.-W.; Li, Q.-S.; Xu, F.-B.; Song, H. B.; Zhang, Z.-Z. *Eur. J. Org. Chem.* **2006**, 1310−1316.
(19) Gil-Rubio, J.; Cámara, V.; Bautista, D.; Vicente, J. *Inorg. Chem.* **2013**, *52*, 4071−4083.
(20) (a) Fränkel, R.; Kniczek, J.; Ponikwar, W.; Nöth, H.; Polborn, K.; Fehlhammer, W. P. *Inorg. Chim. Acta* **2001**, *312*, 23−39. (b) Papini, G.; Bandoli, G.; Dolmella, A.; Gioia Lobbia, G.; Pellei, M.; Santini, C. *Inorg. Chem. Commun.* **2008**, *11*, 1128−1131.
(21) (a) Barnard, P. J.; Baker, M. V.; Berners-Price, S. J.; Skelton, B. W.; White, A. H. *Dalton Trans.* **2004**, 1038−1047. (b) Barnard, P. J.; Wedlock, L. E.; Baker, M. V.; Berners-Price, S. J.; Joyce, D. A.; Skelton, B. W.; Steer, J. H. *Angew. Chem., Int. Ed.* **2006**, *45*, 5966−5970. (c) Wedlock, L. E.; Aitken, J. B.; Berners-Price, S. J.; Barnard, P. J. *Dalton Trans.* **2013**, *42*, 1259−1266.
(22) Wang, J. W.; Song, H.-B.; Li, Q.-S.; Xu, F.-B.; Zhang, Z.-Z. *Inorg. Chim. Acta* **2005**, *358*, 3653−3658.
(23) Liu, A.; Zhang, X.; Chen, W.; Qiu, H. *Inorg. Chem. Commun.* **2008**, *11*, 1128−1131.
(24) (a) dit Dominique, F. J.-B.; Gornitzka, H.; Sournia-Saquet, A.; Hemmert, C. *Dalton Trans.* **2009**, 340−352. (b) Cure, J.; Poteau, R.; Gerber, I. C.; Gornitzka, H.; Hemmert, C. *Organometallics* **2012**, *31*, 619−626.
(25) Carcedo, C.; Knight, J. C.; Pope, S. J. A.; Fallis, I. A.; Dervisi, A. *Organometallics* **2011**, *30*, 2553−2562.
(26) (a) Baron, M.; Tubaro, C.; Biffis, A.; Basato, M.; Graiff, C.; Poater, A.; Cavallo, L.; Armaroli, N.; Accorsi, G. *Inorg. Chem.* **2012**, *51*, 1778−1784. (b) Tubaro, C.; Baron, M.; Costante, M.; Basato, M.; Biffis, A.; Gennaro, A.; Isse, A. A.; Graiff, C.; Accorsi, G. *Dalton Trans.* **2013**, *42*, 10952−10963. (c) Biffis, A.; Cipani, M.; Tubaro, C.; Basato, M.; Costante, M.; Bressan, E.; Venzo, A.; Graiff, C. *New J. Chem.* **2013**, *37*, 4176−4184.
(27) (a) Gierz, V.; Maichle-Mössmer, C.; Kunz, D. *Organometallics* **2012**, *31*, 739−747. (b) Gierz, V.; Seyboldt, A.; Maichle-Mössmer, C.; Törnroos, K. W.; Speidel, M. T.; Speiser, B.; Eichele, K.; Kunz, D. *Organometallics* **2012**, *31*, 7893−7901.
(28) Poethig, A.; Strassner, T. *Organometallics* **2012**, *31*, 3431−3434.
(29) (a) Hahn, F. E.; Radloff, C.; Pape, T.; Hepp, A. *Chem.—Eur. J.* **2008**, *14*, 10900−10904. (b) Rit, A.; Pape, T.; Hahn, F. E. *Organometallics* **2011**, *30*, 6393−6401. (c) Schulte to Brinke, C.; Pape, T.; Hahn, F. E. *Dalton Trans.* **2013**, *42*, 7330−7337. (d) Han, Y.-F.; Jin, G.-X.; Hahn, F. E. *J. Am. Chem. Soc.* **2013**, *135*, 9263−9266.
(30) (a) Hu, X.; Castro Rodriguez, I.; Olsen, K.; Meyer, K. *Organometallics* **2004**, *23*, 755−764. (b) Zhou, Y.; Chen, W. *Organometallics* **2007**, *26*, 2742−2746. (c) Biffis, A.; Gioia Lobbia, G.; Papini, G.; Pellei, M.; Santini, C.; Scattolin, E.; Tubaro, C. *J. Organomet. Chem.* **2008**, *693*, 3760−3766. (d) Rit, A.; Pape, T.; Hahn, F. E. *J. Am. Chem. Soc.* **2010**, *132*, 4572−4573.
(31) (a) Schmidbaur, H.; Schier, A. *Chem. Soc. Rev.* **2008**, *37*, 1931−1951. (b) Schmidbaur, H.; Schier, A. *Chem. Soc. Rev.* **2012**, *41*, 370−412.
(32) (a) Schmidbaur, H.; Graf, W.; Müller, G. *Angew. Chem., Int. Ed. Engl.* **1988**, *27*, 417−419. (b) Narayanaswamy, R.; Young, M. A.; Parkhurst, E.; Ouellette, M.; Kerr, M. E.; Ho, D. M.; Elder, R. C.; Bruce, A. E.; Bruce, M. R. M. *Inorg. Chem.* **1993**, *32*, 2506−2517. (c) Deák, A.; Megyes, T.; Tárkányi, G.; Király, P.; Biczók, L.; Pálinkás, G.; Stang, P. J. *J. Am. Chem. Soc.* **2006**, *128*, 12668−12670.
(33) (a) Vogler, A.; Kunkely, H. *Coord. Chem. Rev.* **2001**, *219−221*, 489−507. (b) Yam, V. W.-W.; Cheng, E. C.-C. *Top. Curr. Chem.* **2007**, *281*, 269−309. (c) Yam, V. W.-W.; Cheng, E. C.-C. *Chem. Soc. Rev.* **2008**, *37*, 1806−1813. (d) He, X.; Yam, V. W.-W. *Coord. Chem. Rev.* **2011**, *255*, 2111−2123. (e) Lima, J. C.; Rodríguez, L. *Chem. Soc. Rev.* **2011**, *40*, 5442−5456. (f) Visbal, R.; Ospino, I.; López-de-Luzuriaga, J. M.; Laguna, A.; Gimeno, M. C. *J. Am. Chem. Soc.* **2013**, *135*, 4712−4715.
(34) (a) Rodríguez, L.; Ferrer, M.; Crehuet, R.; Anglada, J.; Lima, J. C. *Inorg. Chem.* **2012**, *51*, 7636−7641. (b) Visbal, R.; Gimeno, M. C. *Chem. Soc. Rev.* **2014**, *43*, 3551−3574.
(35) (a) Rios, D.; Pham, D. M.; Fettinger, J. C.; Olmstead, M. M.; Balch, A. L. *Inorg. Chem.* **2008**, *47*, 3442−3451. (b) Saitoh, M.; Balch, A. L.; Yuasa, J.; Kawai, T. *Inorg. Chem.* **2010**, *49*, 7129−7134.
(36) Okuyama, K.; Sugiyama, J.; Nagahata, R.; Asai, M.; Ueda, M.; Takeuchi, K. *J. Mol. Catal. A: Chem.* **2003**, *203*, 21−27.
(37) Ito, K.; Nishina, N.; Ohno, H. *Electrochim. Acta* **2000**, *45*, 1295−1298.
(38) Budzelaar, P. H. M. *gNMR*, version 5.1, 1995.
(39) Pyykkö, P. *Chem. Soc. Rev.* **2008**, *37*, 1967−1997.
(40) (a) Baldes, A.; Weigend, F. *Mol. Phys.* **2013**, *111*, 2617−2624. (b) Weigend, F.; Evers, F.; Weissmüller, J. *Small* **2006**, *2*, 1497−1503.
(41) (a) Ahlrichs, R.; Bär, M.; Häser, M.; Horn, H.; Kölmel, C. *Chem. Phys. Lett.* **1989**, *162*, 165−169. (b) Furche, F.; Ahlrichs, R.; Hättig, C.; Klopper, W.; Sierka, M.; Weigend, F. *WIREs Comp. Mol. Sci.* **2014**, *4*, 91−100. (c) Eichkorn, K.; Treutler, O.; Oehm, H.; Haeser, M.; Ahlrichs, R. *Chem. Phys. Lett.* **1995**, *242*, 652−660. (d) Treutler, O.; Ahlrichs, R. *J. Chem. Phys.* **1995**, *102*, 346. (e) Arnim, M. v.; Ahlrichs, R. *J. Comput. Chem.* **1998**, *19*, 1746. (f) Eichkorn, K.; Weigend, F.; Treutler, O.; Ahlrichs, R. *Theor. Chem. Acc.* **1997**, *97*, 119. (g) *TURBOMOLE*, V6.4 2012, a development of University of Karlsruhe and Forschungszentrum Karlsruhe GmbH, 1989−2007, Turbomole GmbH since 2007, available from http://www.turbomole.com.
(42) (a) Dirac, P. A. M. *Proc. R. Soc. (London) A* **1929**, *123*, 714. (b) Slater, J. C. *Phys. Rev.* **1951**, *81*, 385. (c) Vosko, S. H.; Wilk, L.; Nusair, M. *Can. J. Phys.* **1980**, *58*, 1200. (d) Becke, A. D. *Phys. Rev. A* **1988**, *38*, 3098. (e) Perdew, J. P. *Phys. Rev. B* **1986**, *33*, 8822.
(43) Grimme, S. *J. Comput. Chem.* **2006**, *27*, 1787.
(44) Lee, C.; Yang, W.; Parr, R. G. *Phys. Rev. B* **1988**, *37*, 785.
(45) (a) Perdew, J. P.; Wang, Y. *Phys. Rev. B* **1992**, *45*, 13244. (b) Perdew, J. P.; Burke, K.; Ernzerhof, M. *Phys. Rev. Lett.* **1996**, *77*, 3865.
(46) Tao, J.; Perdew, J. P.; Staroverov, V. N.; Scuseria, G. E. *Phys. Rev. Lett.* **2003**, *91*, 146401.
(47) Grimme, S.; Antony, J.; Ehrlich, S.; Krieg, H. *J. Chem. Phys.* **2010**, *132*, 154104.
(48) (a) Weigend, F. *Phys. Chem. Chem. Phys.* **2006**, *8*, 1057. (b) Weigend, F.; Ahlrichs, R. *Phys. Chem. Chem. Phys.* **2005**, *7*, 3297.
(49) Andrae, D.; Haeussermann, U.; Dolg, M.; Stoll, H.; Preuss, H. *Theor. Chim. Acta* **1990**, *77*, 123−141.

DOI: 10.1021/ic502751s
Inorg. Chem. 2015, 54, 6100−6111